Semiquantitative Assessment of Myocardial Blood Flow and Viability Using Polar Map Displays of Cardiac PET Images

Gerold Porenta, William Kuhle, Johannes Czernin, Osman Ratib, Richard C. Brunken, Michael E. Phelps, and Heinrich R. Schelbert

Division of Nuclear Medicine and Biophysics, Department of Radiological Sciences, UCLA School of Medicine University of California, Los Angeles, California and Laboratory of Nuclear Medicine, Laboratory of Biomedical and Environmental Sciences, University of California, Los Angeles, California*

Preserved glucose metabolism in ischemically injured, dysfunctional myocardial tissue as demonstrated on PET imaging predicts functional improvement after revascularization. To characterize more precisely the relationship between regional myocardial blood flow, viability and extent and severity of flow and metabolism abnormalities, we developed a PC-based semiquantitative analysis technique using ^{13}N-ammonia and ^{18}F-deoxyglucose polar map displays. A data base for mean values (m) and standard deviations (s.d.) for relative ^{13}N activities reflecting regional myocardial blood flow, relative ^{18}F activities normalized to normal flow regions reflecting regional glucose utilization and the difference of normalized ^{18}F and ^{13}N activities as an index of a flow-metabolism mismatch was established in 11 normals. Parametric polar maps were derived by comparing patient data to a normal range defined as >m − 2 s.d. for relative myocardial blood flow and <m + 2 s.d. for both relative glucose utilization and the difference between normalized ^{18}F and ^{13}N activities. Semiquantitative indices of extent and severity of blood flow defects, of relative increases in glucose utilization and of flow-metabolism mismatch areas are generated for the entire myocardium and the three coronary territories. The approach promises to be clinically useful to confirm presence and absence of flow and metabolic abnormalities and to assess their extent as a potential predictor of functional outcome after therapy.

J Nucl Med 1992; 33:1623–1631

Positron emission tomography (PET) of myocardial blood flow and glucose utilization identifies viable myocardium (*1,2*). A blood flow-metabolism mismatch, defined as an increase in glucose utilization relative to blood flow, predicts an improvement in contractile function following revascularization (*1,2*). Furthermore, earlier observations suggest that the geographic extent of a blood flow-metabolism mismatch may predict the magnitude of an improvement in global left ventricular function following surgical revascularization (*1*). Previous studies determined the extent and severity of regional disparities between blood flow and glucose utilization by visual inspection or by circumferential profile analysis of transaxially acquired PET images. However, the accuracy and reproducibility of these analytic approaches are limited because of variations in cardiac size and orientation within the chest which can cause artifactual alterations in regional tracer concentrations on transaxial images.

State-of-the-art, high spatial resolution, multiplane PET scanners overcome these limitations for they permit the reorientation of transaxial images into short-axis slices that can be assembled into polar map displays independent of the heart's orientation in the chest cavity (*3–5*). Semiquantitative analysis methods, as, for example, circumferential activity profiles that are frequently used for the analysis of SPECT images to compare patient data to a data base established from normal volunteers, can be applied to reduce variability due to subjective visual interpretation. In order to delineate more accurately the distribution of blood flow and glucose utilization throughout the left ventricular myocardium, we developed a semiquantitative analysis technique for mapping the geographic extent and severity of flow defects, of relative increases in glucose utilization and of flow-metabolism mismatches in the entire left ventricular myocardium and in the territories of the three major coronary arteries.

MATERIALS AND METHODS

PET Image Acquisition

Nitrogen-13-ammonia and ^{18}F-deoxyglucose were used as tracers of myocardial blood flow and glucose utilization. Fifteen transaxial images, spaced apart by 6.5 mm, were acquired simultaneously with a high spatial resolution PET scanner (ECAT 931; CTI/Siemens, Knoxville, TN; intrinsic resolution of 6 mm FWHM). A 20-min transmission scan was obtained first for attenuation correction. Nitrogen-13-ammonia (10–15 mCi) was

Received Jan. 7, 1992; revision accepted May 5, 1992.

For reprints contact: Heinrich R. Schelbert, MD., Division of Nuclear Medicine and Biophysics, UCLA School of Medicine, Los Angeles, CA 90024-1721.

* Operated for the U.S. Department of Energy by the University of California under contract #DE-FC03-87ER60615.

then injected intravenously and, 5 min later, a 20-min image of the myocardial ^{13}N activity was obtained. Forty to 50 min later, ^{18}F-deoxyglucose (10 mCi) was injected intravenously and after 40 min, a 20-min image of the myocardial ^{18}F activity was acquired. To improve the quality of the myocardial ^{18}F-deoxyglucose images (*6*), glucose (Trutol, 100g) was given orally at the time of the transmission scan, that is, 1 hr prior to the ^{18}F-deoxyglucose administration.

Image Analysis and Display

The transaxial images were reconstructed on a dedicated minicomputer (microVAX, Digital Equipment Corp., Maynard, MA) into 128 × 128 image matrices with a pixel size of 1.5 × 1.5 mm using a Shepp 0.15 filter. The final in-plane image resolution was 10.3 mm FWHM. The transaxial images were transferred to a low-cost desktop personal workstation with an 8-bit color display (Macintosh IIcx, Apple Computer Inc., Cupertino, CA). The CALIPSO software package for medical image processing (*7*) was expanded by software modules written in C (Think C, Symantec Corp., Cupertino, CA) for reorientation of the transaxial into short axis images and to generate and analyze polar map displays.

Due to the physical design of the scanner used in this study, acquisition of the image data is inhomogeneous with respect to the three spatial dimensions. Specifically, the in-plane resolution, which depends on detector design and reconstruction filters, differs from the axial resolution, which primarily depends upon plane spacing. Possible effects of the heterogeneous data sampling on the resliced images, e.g., distortion due to the reorientation algorithms, have been characterized in phantom experiments (*8*). A hybrid interpolation algorithm with linear interpolation in-plane and cubic interpolation between planes was therefore developed as reslicing algorithm. When compared to a simpler interpolation scheme using linear interpolation in-plane and between planes, the hybrid interpolation algorithm proved to be superior with respect to count recovery and geometric distortions (*8*). The Macintosh IIcx computer model (68020 processor, 16 MHz clock speed) allows reorientation of 15 transaxial 128 × 128 8-bit pixel planes into 6 100 × 100 8-bit pixel short-axis planes in approximately 1 min. Interactive determination of reorientation parameters is operator dependent and can be as short as 30 sec.

Six short-axis planes reaching from the endocardial border of the apex to the base of the left ventricle were used (Fig. 1, see page 1634). While the reslicing algorithm allows an increase in the spatial density of images by generating more than six short-axis planes, image resolution is primarily determined by plane thickness and interplane spacing of the originally acquired transaxial images. With the tomograph used in this study, the left ventricular myocardium is usually depicted on a set of six to eight contiguous transaxial images. While some gain in the accuracy of delineating extent and severity might be possible with a greater number of planes, especially in instances of left ventricular enlargement, this gain would be anticipated to be rather small. Even in large left ventricles with a larger interplane spacing, interplane defects would be extrapolated and thus would be sufficiently well reflected on the polar maps. Thus, depiction of the left ventricular myocardium in six distinct short-axis slices was considered sufficient for clinical image analysis that focuses primarily on the assessment of regional myocardial blood flow and metabolism in anatomical segments and vascular territories. Polar maps were generated from circumferential profiles of the maximal regional myocardial count activity obtained along 60 equally spaced radial profiles which were constrained by elliptic regions of interest encompassing the left ventricular myocardium on the six short-axis cross sections. The polar maps assembled from short-axis images do not include tracer activity distributions in the apex of the left ventricle. While the display may therefore miss small apical abnormalities of myocardial blood flow and metabolism, the clinical relevance of abnormalities confined to the apex remains undetermined. Also, apical count activity is severely affected by partial volume effects and thus difficult to analyze.

These "raw" polar maps assembled from the reoriented ^{13}N-ammonia and the ^{18}F-deoxyglucose images were subsequently normalized to allow comparison to the normal data base. Assuming that the regions on the polar maps with the highest ^{13}N activity concentrations corresponded to normally perfused myocardium, pixel values in the top 5% of the raw polar map were averaged to obtain the normalization factor for the ^{13}N-ammonia images. For display purposes, the maximal pixel value of the normalized ^{13}N polar map was set to a value of 250. This particular normalization procedure was preferred over normalization by maximal count rate as it attenuates the influence of outliers and thus is less susceptible to normalization distortions.

A similar approach was used to generate normalized polar maps for ^{18}F-deoxyglucose. Assuming that glucose metabolism is normal in myocardial regions with normal blood flow, the ^{18}F pixel values in those myocardial regions with relative ^{13}N activity concentrations above 95% were averaged and a "reference" normalization factor was obtained. Normalization was then performed analogous to the ^{13}N ammonia polar map procedure. This approach assumes that glucose metabolism is always normal in normally perfused myocardium. One can, however, envision one situation when blood flow is normal but ^{18}F-deoxyglucose may be abnormal: stunned myocardium. However, the impaired wall motion in these cases would result in an apparent partial volume related flow reduction. To accommodate both regional increases and decreases of ^{18}F activity concentrations on the polar and map displays using the same color code, ^{18}F pixel values equal to the normalization factor were assigned a pixel value of 125 (i.e., 50% of the maximal normal ^{13}N activity).

Normalization of raw^{18}F polar maps delineates areas with increased or decreased glucose utilization. Because the approach, per se, does not identify increases in glucose metabolism relative to blood flow, the normalized polar maps for ^{18}F-deoxyglucose were compared to those for ^{13}N-ammonia uptake, resulting in a "difference polar map." This was accomplished by encoding the differences between the regional ^{18}F and ^{13}N counts (F-N) in an additional polar map based on a simple pixel-by-pixel computation as described by F-N = 2*(F-18) − (N-13) + 125. The approach assigns to myocardial regions with matching ^{18}F and ^{13}N counts a pixel value of 125 (green on the color scale), while regions with relative increases or decreases in ^{18}F counts appear brighter (yellow, red) or darker (blue, black), respectively. The pixel difference of normalized ^{18}F and ^{13}N counts rather than their ratio was used to compute an index of blood flow-metabolism mismatch. Differences are less susceptible than ratios to measurement errors. Although measurement errors may be small in absolute terms, they would be augmented by ratios and disproportionately bias the results of the semiquantitative analysis method.

Generation of Normal Data Bases and "Parametric" Polar Maps

A normal range for the distributions of ^{13}N-ammonia and ^{18}F-deoxyglucose concentrations was established in 11 volunteers who were at low risk for coronary artery disease as determined by age (mean: 24 yr, range: 18–37 yr), history, electrocardiography and risk factors. None of the subjects had diabetes mellitus. Each volunteer signed an informed consent form as approved by the UCLA Human Subject Protection Committee before being studied with ^{13}N-ammonia and ^{18}F-deoxyglucose on PET.

Images in the normal volunteers were acquired and analyzed as outlined above and three sets of 11 normalized polar maps were obtained. Average pixel values (m) and standard deviations (s.d.) were determined separately for each of the three polar maps (the ^{13}N activity, the ^{18}F activity, the difference polar map) and assembled into data bases that were then used for defining the normal ranges on a pixel-by-pixel basis. For the ^{13}N-ammonia polar map of myocardial blood flow, pixel values above m − 2 s.d. were considered normal. For the ^{18}F-deoxyglucose polar map of relative glucose utilization and for the difference map, a pixel range between m + s.d. and m − 2 s.d. was defined as the normal range.

To delineate more quantitatively the relative distributions of blood flow and glucose metabolism in patients, color-coded polar maps were created that compare blood flow and metabolism to the normal data base and depict the extent and magnitude of blood flow and metabolism abnormalities by different color gradations. Seven colors were selected (bright red, dark red, yellow, green, magenta, blue and violet) and assigned to each pixel in the color-coded polar map according to the degree of deviation from the normal range. For the blood flow polar map, m − 2 s.d. as the lower limit of normal was assigned a relative value of 100% and six colors from dark red to violet were used to depict zones of decreasing blood flow (dark red > 100% > yellow > 80% > green > 60% > magenta >40% > blue > 20% > violet). For the ^{18}F-deoxyglucose and for the difference polar maps, seven colors were used to delineate the relation of patient data to the normal range as follows: bright red > m + 3 s.d. > dark red > m + 2 s.d. > yellow > m + 1 s.d. > green > m − 1 s.d. > magenta > m − 2 s.d. > blue > m − 3 s.d. > violet.

The entire left ventricular myocardium or the territories of the three major coronary arteries (left anterior descending, left circumflex and right coronary artery) were analyzed for extent and severity of abnormal blood flow and glucose utilization. The assignment of the vascular territories to the polar map was adopted from the vascular distribution established in stress-rest SPECT ^{201}Tl studies (*9*) because a sufficient number of single-vessel disease patients for delineation of vascular territories on PET images was not yet available. The geographic extent of an abnormality was estimated from the fraction of pixel values either below the normal range for blood flow or above the normal range for glucose utilization and the ^{18}F − ^{13}N difference for the entire left ventricle and for each vascular territory.

Geometric distortions due to mapping of the three-dimensional myocardial tracer distribution onto two-dimensional polar maps may bias the computation of geometric fractions. To reduce the effects of distortions on the indices describing the geometric extent and severity of abnormalities, a correction method was developed to adjust for the tapering of the left ventricular radius from the base to the apex that is independent of the computer display format of the polar maps. Correction factors of mean relative left ventricular diameters were derived for each short-axis plane (1, 0.99, 0.94, 0.87, 0.76, 0.61 for planes 1 to 6 proceeding from the base to the apex) by a previously validated method for measuring the mean left ventricular radius in each plane in the 11 normals (*10*). Semiquantitative indices were then determined as weighted sums of pixel values employing the appropriate correction factors for each plane. No corrections were made for distortions in relative count rates due to differences between axial and in-plane spatial resolutions of the PET scanner or due to differences in reorientation angles of the left ventricular axis. These effects have previously been characterized in detail (*8*) and were considered of minor importance for the present study.

The severity of abnormalities in tracer uptake was assessed by computing the average percent reduction (units: %) of the relative myocardial ^{13}N-ammonia uptake below the lower limit of normal, m − 2 s.d., or the average fractional increase of the relative myocardial ^{18}F activity or the ^{18}F to ^{13}N difference (units: s.d.) above the upper limit of normal, m + 2 s.d. Again, these indices were corrected for geometric distortions as detailed above.

To examine the homogeneity of myocardial ^{13}N and ^{18}F activity and their difference, mean values and standard deviations of normalized tracer activities were determined in six anatomical regions (anterior, lateral, posterolateral, inferior, posteroseptal, anteroseptal). These regions were assigned to six contiguous 60° sectors on the polar maps starting from the anterior insertion of the right ventricle (10 o'clock on the polar map) and proceeding clockwise around the full circle.

Initial Evaluation of Polar Map Approach in Normals and in Patients

The new polar map approach and its ability to delineate abnormal patterns of blood flow and metabolism was then tested in five additional normal volunteers (Table 2A) and in 10 non-diabetic patients with arteriographically documented coronary artery disease. Eight patients had chronic stable coronary artery disease with >70% luminal diameter stenosis of at least one major coronary artery. Two patients were studied within 72 hr after an acute myocardial infarction (Table 2B).

RESULTS

Tables 1A and B present the distribution of mean values and standard deviations of relative ^{13}N and ^{18}F activities and their difference for six myocardial segments, three vascular territories and the entire left ventricular myocardium for the 11 normal volunteers. Because the normalization algorithm is based on the myocardial distribution of ^{13}N activities, relative values of ^{13}N activities are by definition lower than 100%. Thus, average values for ^{13}N activities are lower than average ^{18}F activities. The homogeneity of values was analyzed by ANOVA with Scheffe's test for multiple comparisons. Differences were considered significant if the probability of a type I error was less than 1%.

The relative concentrations of the ^{13}N activity differed significantly between myocardial segments defined by both anatomical and vascular classification criteria. Most prominent was a decrease of the mean values in the lateral, posterolateral, and inferior segments of the left ventricle.

TABLE 1A
Distribution of Relative Regional Mean Values of Normalized ^{13}N and ^{18}F Activities and Their Difference (F-N) in 11 Normal Subjects

	^{13}N	p	^{18}F	p	F-N	p
Total	80 ± 8		93 ± 7		13 ± 8	
Vascular territories						
LAD (1)	82 ± 7	all	94 ± 5	—	12 ± 5	all
CX (2)	72 ± 5	all	94 ± 6	—	22 ± 6	all
RCA (3)	86 ± 6	all	92 ± 8	—	6 ± 6	all
Segments						
Anterior (1)	83 ± 6	2, 3	95 ± 4	5	12 ± 5	3, 4, 5
Lateral (2)	76 ± 4	all	91 ± 4	4	15 ± 4	3, 5, 6
Posterolateral (3)	71 ± 5	all	93 ± 6	4	22 ± 5	1, 2, 5, 6
Inferior (4)	80 ± 7	2, 3, 5, 6	98 ± 8	2, 3, 5	18 ± 10	1, 5, 6
Posteroseptal (5)	86 ± 6	2, 3, 4	90 ± 7	1, 4, 6	4 ± 4	all
Anteroseptal (6)	86 ± 6	2, 3, 4	95 ± 7	5	10 ± 2	2, 3, 4, 5

Values given are % ± s.d. of the normalization factor for ^{13}N and ^{18}F activities and the percent difference for F-N. Numeric references to vascular territories or segments that reach on pairwise comparisons statistical significance based on an ANOVA with Scheffe test ($p < 0.01$) are listed in the respective p column.

Standard deviations as a measure of the variability in tracer uptake in normal subjects were also increased in these segments. Thus, polar maps of the relative distribution of ^{13}N activity in left ventricular myocardium derived by thresholding normalized polar maps against a fixed lower limit would lead to a higher false-positive rate for detection of blood flow defects in the lateral, posterolateral and inferior segments. Therefore, the relative ^{13}N activity concentrations must be compared to a normal data base that accounts for regional heterogeneities in tracer uptake in a population of normals.

In contrast, myocardial ^{18}F activity concentrations were more homogeneous. There were no statistically significant differences between vascular territories. The range of segmental mean values of 8% (inferior versus posteroseptal) was smaller than the range of 15% (anteroseptal versus posterolateral) for the mean segmental ^{13}N activity.

Nevertheless, in 15 paired comparisons between anatomic segments, five pairs involving either the inferior or the posteroseptal segments reached statistical significance. Also, the standard deviations about the mean in the lateral, posterolateral and inferior wall were higher than in the remaining myocardial segments. Therefore, a comparison of ^{18}F activity concentrations to a normal data base is similarly preferable over fixed thresholding for detection of regional abnormalities in ^{18}F-deoxyglucose uptake. However, the difference between the fixed thresholding and the comparison to a normal data base will be less for ^{18}F-deoxyglucose than for the ^{13}N-ammonia images.

The variability of regional ^{13}N activity concentrations resulted in a significant variability in the regional differences between ^{18}F and ^{13}N counts. This difference was highest in the posterolateral wall. On the other hand, the standard deviations were homogeneous. Therefore, polar maps of the regional differences between ^{13}N and ^{18}F activities required the development of an algorithm for comparison of the regional count differences to a data base of normal.

TABLE 1B
Distribution of Relative Regional Standard Deviations of Normalized ^{13}N and ^{18}F Activities and Their Difference (F-N) in 11 Normal Subjects

	^{13}N	p	^{18}F	p	F-N	p
Total	6.7 ± 1.8		11.3 ± 2.4		11.7 ± 2.2	
Vascular territories						
LAD (1)	5.8 ± 1.5	all	10.2 ± 2.7	2	11.5 ± 2.5	—
CX (2)	8.1 ± 1.4	all	12.7 ± 1.5	all	11.1 ± 1.7	—
RCA (3)	6.5 ± 1.8	all	10.9 ± 2.1	2	11.8 ± 2.5	—
Segments						
Anterior (1)	5.6 ± 1.4	2, 3, 4	9.7 ± 2.8	2, 3, 4	11.4 ± 2.8	—
Lateral (2)	6.8 ± 1.4	1, 3	12.4 ± 2.0	1, 5, 6	11.9 ± 1.4	—
Posterolateral (3)	8.3 ± 1.3	1, 2, 5, 6	12.3 ± 1.3	1, 5, 6	10.6 ± 1.6	4
Inferior (4)	7.7 ± 1.6	1, 5, 6	12.2 ± 1.6	1, 6	12.9 ± 2.2	3
Posteroseptal (5)	6.1 ± 1.8	3, 4	10.7 ± 2.1	2, 3	11.5 ± 2.3	—
Anteroseptal (6)	5.9 ± 1.7	3, 4	10.5 ± 2.6	2, 3, 4	11.7 ± 2.3	—

Notations as in Table 1A.

Tables 2 and 3 list the observations with the polar map analysis in 5 normals and 10 patients. In the normal subjects, the extent of blood flow defects averaged 5.9%. This value did not differ significantly from the 2.5% expected theoretically from the definition of the normal range by two standard deviations. The severities of blood flow defects ranged from 0 to 8% and averaged 2.7%. In the patients, the extent of flow defects in vascular territories subtended by a coronary artery with a <70% (n = 8) or ≥70% (n = 22) diameter stenosis averaged 29% and 63% while the corresponding defect severities averaged 16% and 30%. Only the values for the vascular territories subtended by arteries with a ≥70% stenosis were larger than the values in the normal subjects. Moreover, defect extent but not defect severity differed significantly between the two groups of patients (ANOVA with Scheffe test, $p < 0.01$).

In vascular territories supplied by a vessel with a ≥70% luminal stenosis, the severity of blood flow defects did not correlate with the extent of viable myocardium as assessed by elevated F-N values ($r = 0.12$, p = n.s.). Also, there was no statistically significant correlation between the extent of flow defects and the extent of blood flow-metabolism mismatches ($r = 0.30$, p = n.s.).

Figure 2 shows short-axis images of myocardial ^{13}N and ^{18}F uptake and polar maps in a normal subject (ID 2403). While the short-axis images and normalized polar maps are displayed in a full 8-bit color scale with 255 different colors, the polar maps indicating the degree of deviation from normal use a reduced color scheme with only six ^{13}N or seven (^{18}F, $^{18}F - ^{13}N$) different color levels. As expected in a normal subject, myocardial ^{13}N and ^{18}F activities show only minor abnormalities as assessed by polar map analysis.

Figures 3 and 4 show polar maps in two patients with coronary artery disease. The patient shown in Figure 3 had an extensive anterior myocardial infarction (Patient 2533 in Table 2B), a complete occlusion of the left anterior descending coronary artery and a left ventricular ejection fraction of only 17%. The ^{13}N-ammonia polar map reveals an extensive blood flow defect in the left anterior descending territory extending to the apex and inferoapical wall. The ^{18}F-deoxyglucose polar map depicts a metabolic abnormality that parallels in extent and severity the flow defect. The difference polar map therefore does not demonstrate a regionally increased count difference or evidence of a blood flow-metabolism mismatch. The patient shown in Figure 4 (#50187) had severe triple-vessel disease, left main stenosis and a left ventricular ejection fraction of only 13%. The polar maps demonstrate an extensive blood flow-metabolism mismatch that occupies nearly 50% of the left ventricular myocardium. Thus, both patients had comparable flow defects and equally depressed left ventricular function. The ^{18}F-deoxyglucose and the difference polar maps indicate marked differences, however, in the degree of the ischemic injury. The extensive blood flow-metabolism mismatch in the second patient predicts a significant post-revascularization improvement in the left

TABLE 2A
Regional Relative Myocardial ^{13}N and ^{18}F Activities and Their Difference in Entire Myocardium and Three Vascular Territories Derived From Parametric Polar Map Analysis in Five Normal Subjects

				^{13}N		^{18}F		F-N	
Volunteer	Age	Sex	Territory	Ext. (%)	Sev. (%)	Ext. (%)	Sev. (s.d.)	Ext. (%)	Sev. (s.d.)
2339	19	M	Tot	8	4	1	1.3	0	0.0
			LAD	1	3	4	1.3	0	0.0
			CX	8	8	0	0.0	0	0.0
			RCA	11	2	0	0.0	0	0.0
2372	23	M	Tot	9	4	5	0.5	13	0.6
			LAD	7	1	0	0.0	0	0.0
			CX	15	6	4	0.2	29	0.6
			RCA	5	2	13	0.6	11	0.6
2374	25	M	Tot	2	5	4	1.8	7	0.9
			LAD	0	0	8	2.6	9	1.5
			CX	0	0	0	0.0	0	0.0
			RCA	8	5	4	0.9	14	0.6
2403	19	M	Tot	5	5	1	0.1	0	0.0
			LAD	0	0	0	0.0	0	0.0
			CX	3	4	0	0.0	0	0.0
			RCA	8	3	2	0.2	0	0.0
2405	21	M	Tot	7	4	0	0.0	1	0.4
			LAD	0	0	1	0.1	0	0.0
			CX	17	6	0	0.0	3	0.5
			RCA	6	1	0	0.0	1	0.2

Tot = entire myocardium; LAD = left anterior descending artery; CX = circumflex artery; and RCA = right coronary artery.

TABLE 2B

Regional Relative Myocardial ^{13}N and ^{18}F Activities and Their Difference (F-N) in Entire Myocardium and Three Vascular Territories Derived from Parametric Polar Map Analysis in 10 Patients with Angiographically Proven Coronary Artery Disease

				^{13}N		^{18}F		F-N		Angiography	
Patient	Age	Sex	Territory	Ext. (%)	Sev. (%)	Ext. (%)	Sev. (s.d.)	Ext. (%)	Sev. (s.d.)	Sten (%)	EF (%)
2386	53	F	Tot	71	46	0	0.0	18	1.0		35
			LAD	58	30	1	0.1	7	0.5	100	
			CX	57	50	0	0.0	2	0.5	70	
			RCA	100	53	0	0.0	47	1.1	90	
2465	66	M	Tot	42	16	0	0.0	0	0.0		51
			LAD	74	19	0	0.0	0	0.0	75	
			CX	35	14	0	0.0	0	0.0	0	
			RCA	11	8	0	0.0	1	0.5	80	
2497	62	F	Tot	22	35	1	0.3	0	0.0		61
			LAD	0	0	0	0.0	0	0.0	50	
			CX	31	34	3	0.3	0	0.0	99	
			RCA	31	23	0	0.0	0	0.0	80	
2533	49	M	Tot	77	48	3	1.1	4	0.7		17
			LAD	100	61	0	0.0	1	0.2	100	
			CX	55	44	5	0.6	8	0.8	0	
			RCA	66	30	5	1.6	6	0.7	0	
50187	68	M	Tot	71	28	11	1.1	49	2.0		13
			LAD	52	27	11	0.9	36	2.4	90	
			CX	84	26	0	0.0	49	1.0	100	
			RCA	81	27	17	1.2	61	2.0	95	
50192	61	M	Tot	71	41	0	0.0	0	0.0		36
			LAD	70	43	0	0.0	0	0.0	90	
			CX	39	21	0	0.0	0	0.0	50	
			RCA	100	50	0	0.0	0	0.0	100	
50213	52	M	Tot	29	24	10	0.8	20	0.7		25
			LAD	61	31	9	1.2	28	0.8	100	
			CX	8	8	12	0.6	24	0.5	90	
			RCA	16	11	7	0.5	10	1.2	0	
50233	66	M	Tot	52	43	1	0.3	11	0.9		40
			LAD	4	1	0	0.0	0	0.0	50	
			CX	68	28	0	0.0	1	0.1	90	
			RCA	98	54	0	0.0	44	0.9	90	
50295	59	M	Tot	57	12	2	0.5	9	0.8		19
			LAD	74	12	0	0.0	3	0.4	100	
			CX	35	10	0	0.0	0	0.0	100	
			RCA	65	14	8	0.2	28	0.9	80	
50297	71	M	Tot	52	24	0	0.0	0	0.0		20
			LAD	98	32	0	0.0	0	0.0	100	
			CX	23	10	0	0.0	0	0.0	80	
			RCA	19	5	0	0.0	0	0.0	0	

Tot = entire myocardium; LAD = left anterior descending artery; CX = circumflex artery; RCA = right coronary artery; Sten = luminal stenosis of coronary artery; and EF = ejection fraction.

ventricular function while no such improvement would be expected in the first patient.

DISCUSSION

Identification of viable or reversibly dysfunctional myocardium remains of considerable clinical interest (*11,12*). Previous studies demonstrated that blood flow-metabolism mismatch as determined with ^{13}N-ammonia and ^{18}F-deoxyglucose PET imaging is highly predictive of reversible dysfunction (*1,2*). These earlier studies suggested that the fraction of myocardium with a blood flow-metabolism mismatch on PET imaging may predict the degree of improvement in global left ventricular function following revascularization and, possibly, relief of symptoms related to congestive heart failure. These observations support the need for more quantitative analytical tools for determining the extent and magnitude of blood flow-metabolism mismatches.

In the current study, the regional distributions of normalized count activities were initially assumed to be homogeneous. Analysis of variance of segmental mean values and standard deviations in a data base of normal values, however, uncovered significant differences of segmental

TABLE 3

Extent (Ex) and Severity (Sev) of Abnormalities in Relative Myocardial Perfusion, Relative Glucose Utilization and Their Difference Reflecting Blood Flow-Metabolism Mismatches Detected in Vascular Territories of Healthy Volunteers and Patients with Coronary Artery Disease as Documented by Angiography (at least one vessel ≥ 70% stenosis)

	^{13}N		^{18}F		F-N	
	Ex (%)	Sev (%)	Ex (%)	Sev (s.d.)	Ex (%)	Sev (s.d.)
Volunteers (n = 5)						
Normal (n = 30)	5.9 ± 5.5	2.7 ± 2.6	2.4 ± 3.8	0.39 ± 0.73	4.5 ± 8.2	0.27 ± 0.43
Patients (n = 10)						
Sten. < 70% (n = 8)	29.2 ± 23.7	15.8 ± 15.3	2.1 ± 3.0	0.34 ± 0.57	3.0 ± 4.3	0.34 ± 0.49
Sten. ≥ 70% (n = 22)	62.7 ± 29.3*†	29.5 ± 16.3*	2.7 ± 5.1	0.21 ± 0.40	15.1 ± 20.4	0.54 ± 0.66

* $p < 0.01$ vs normal, † $p < 0.01$ vs Sten. < 70% (ANOVA with Scheffe Test).
Vascular territories of patients are divided into two groups according to stenosis severity (<70%, ≥70%). Values given are means ± s.d.

values for mean and standard deviations of the relative ^{13}N-ammonia activity and, to a lesser degree, also for ^{18}F-deoxyglucose. Accordingly, mean values of the relative count difference between ^{18}F and ^{13}N activities also differed between segments. Differences in segmental ^{13}N concentrations existed on the normalized polar maps. Tracer uptake was reduced especially in the lateral and posterolateral segments of the left ventricle. The reason for this heterogeneity remains unexplained. While the possibility of coronary artery disease in the normal volunteers cannot be ruled out entirely, it is unlikely, as these volunteers were young and free of risk factors, and thus had a low probability of coronary artery disease.

While there is no firm evidence to support the notion of physiologically lower blood flows to the posterolateral wall, studies with diffusable inert tracers have suggested the possibility of heterogeneous blood flow in the left ventricular myocardium (*13*). Furthermore, measurements of regional myocardial blood flow with ^{15}O water in humans reported 10%–20% lower values in the lateral and posterior as compared to the septal and anterior segments, although these values failed to achieve statistical significance (*14*). Disproportionately greater wall motion excursions relative to the image plane had been considered as a possible alternate explanation. The normal or even modestly enhanced ^{18}F-deoxyglucose uptake in the same region renders this possibility unlikely. Regardless of the underlying mechanism, the observation implies that reliance on only visual analysis of ^{13}N-ammonia images may cause interpretative errors and supports the need for semiquantitative comparisons to a data base of normal values.

For ^{18}F-deoxyglucose, recent studies using transaxial images demonstrated relative increases in tracer uptake in the posterolateral wall of normal volunteers when studied in the fasted state (*14*). However, the relative tracer uptake becomes more homogeneous and the image quality improves if glucose is administered 1 hr prior to injection of ^{18}F-deoxyglucose. Consistent with these observations (*6*, *14*), the myocardial ^{18}F images obtained in this study after oral glucose loading were of high contrast and exhibited relatively homogeneous ^{18}F-deoxyglucose concentrations. Furthermore, oral glucose loading produces relatively con-

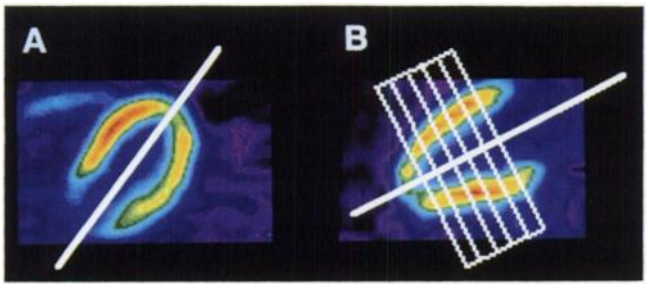

FIGURE 1. Vertical long-axis image of the myocardial ^{18}F activity obtained in a normal subject. The white lines illustrate the location and spacing of six short-axis planes extending from the endocardial border of the apex to the base of the left ventricle. Polar maps are assembled from these short-axis images.

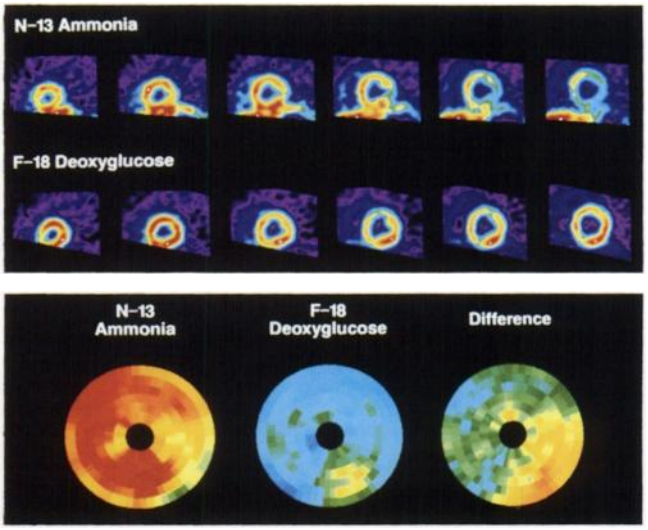

FIGURE 2. (Top) Short-axis images of myocardial ^{13}N and ^{18}F activities reflecting myocardial perfusion and glucose utilization in a normal volunteer (ID 2403). The image planes which depict six myocardial sections from the apex to the base of the left ventricle are oriented as follows: anterior—top, septal—left, inferior—bottom, lateral—right. (Bottom) Normalized polar map displays of the myocardial ^{13}N uptake (left), ^{18}F uptake (center) and the difference polar map (right). Numerical results of a semiquantitative analysis assessing extent and severity of abnormalities are given in Table 2A.

sistent levels of myocardial glucose utilization rates, averaging 0.69 ± 0.11 and 0.80 ± 0.23 μmol/min/g with average intersubject variabilities of 16 and 26% (*15,16*). Consistent with the findings in this study, glucose utilization rates were also observed to be mildly heterogeneous (*15*).

Thus, polar maps of the regional myocardial ^{13}N and ^{18}F concentrations in patients must be compared to polar maps of normals, which accommodate the normal regional variations of mean values and standard deviations and cannot be analyzed by empirical thresholds independent of anatomical location. In addition, normalization of the relative ^{18}F activity concentrations to the distribution of the relative activity concentrations of a flow tracer is critical. As the patient examples in this study demonstrate, viable myocardium is identified more accurately from the difference polar map than from the ^{18}F-deoxyglucose polar map alone.

The present study employed vascular territories established previously for polar map displays of SPECT ^{201}Tl images. The preliminary data in this study demonstrate that these territories generally correspond to myocardium subtended by stenosed coronary arteries. Moreover, anatomical variations in the branching sequence of coronary vessels are frequently observed so that assignments between regions of interest on polar maps and vascular beds can only be approximations. Nevertheless, the accuracy of the vascular territories as assigned to the PET polar maps as well as their clinical utility remain to be validated in a larger group of patients with single-vessel disease. Such validation appears especially important because the accurate correction for photon attenuation of the PET images may eliminate possible geometric distortions inherent to SPECT images. While the initial testing of the polar map approach in patients with ischemic heart disease supports its clinical utility, prospective studies will be needed to validate its accuracy. Equally important will be validation studies in animal experiments with known defect sizes.

In summary, a low cost desktop computer PET image processing software has been developed and evaluated for the generation and analysis of parametric polar maps

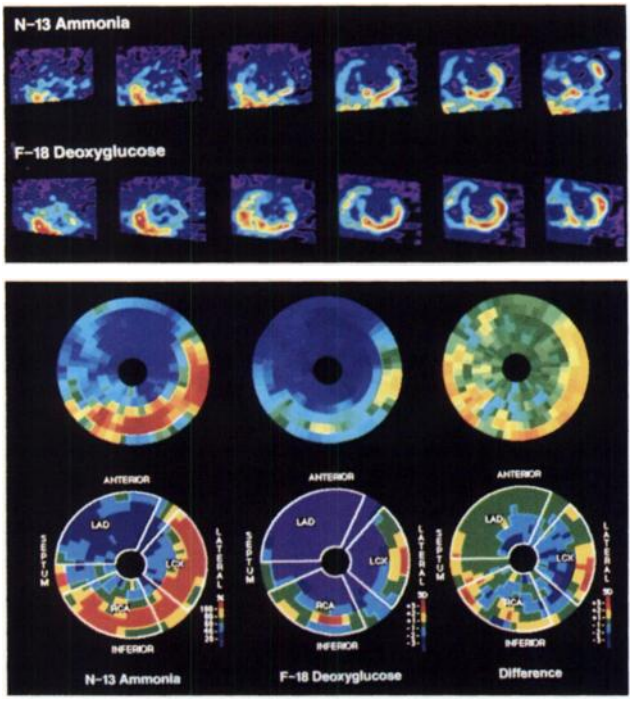

FIGURE 3. (Top) Short-axis images of myocardial ^{13}N and ^{18}F activities obtained in a patient (ID 2533) after an extensive anterior myocardial infarction with complete occlusion of the left anterior descending artery and severely reduced global left ventricular function (ejection fraction: 17%). The perfusion abnormalities delineated on the images of the ^{13}N activity closely match the metabolic abnormalities seen on the ^{18}F images (perfusion/metabolism match). Image are oriented as in Figure 2. (Bottom) The upper row depicts the normalized polar map displays and the lower row the corresponding results of a pixel-by-pixel comparison between normalized polar maps and the data base of normals. Details concerning the color codes are given in the text. Based on the numerical results given in Table 3 confirming the absence of a perfusion/metabolism mismatch, global left ventricular function cannot be expected to improve following revascularization.

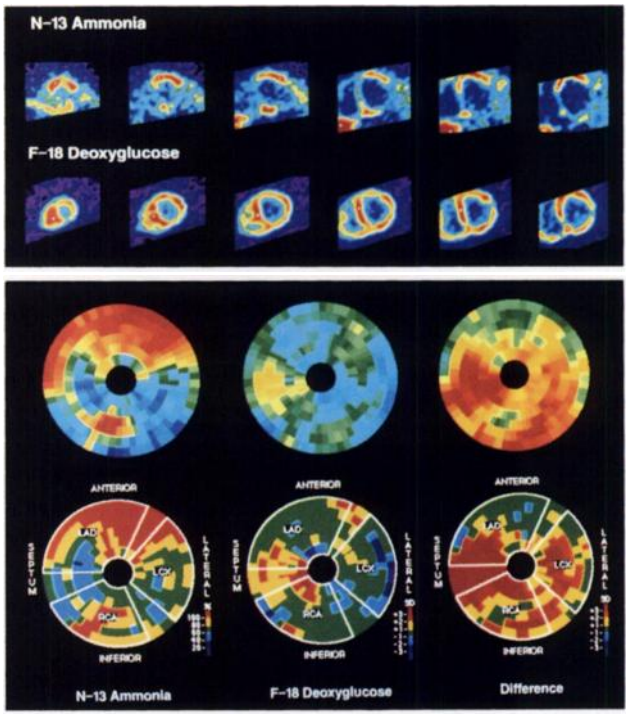

FIGURE 4. (Top) Short-axis images of myocardial ^{13}N and ^{18}F activities obtained in a patient (ID 50187) with severe triple-vessel disease and severely reduced global left ventricular function (ejection fraction: 13%). Large portions of the left and right ventricular myocardium exhibit maintained glucose metabolism in areas with severely reduced myocardial perfusion (perfusion/metabolism mismatch). Images are oriented as in Figure 2. (Bottom) Graphical results of the polar map analysis assessing extent and severity of perfusional and metabolic abnormalities in relation to a normal data base. The numerical results given in Table 3 confirm the presence of an extensive perfusion/metabolism mismatch and suggest the possibility of postinterventional improvement of left ventricular dysfunction after revascularization.

reflecting regional relative myocardial blood flow, glucose utilization and their relationship. While additional prospective studies for further validation would seem warranted, the approach nevertheless should prove useful to confirm presence and extent of viable myocardium after ischemic tissue injury with or without reperfusion attempts.

ACKNOWLEDGMENTS

We thank Ron Sumida, Francine Aguilar, Judy Edwards, Anne Irwin, and Gloria Stocks for their excellent technical assistance, the staff of the Medical Cyclotron at UCLA for providing the isotopes, and Eileen Rosenfeld for her skillful secretarial assistance. This work was supported in part by the Director of the Office of Energy Research, Office of Health and Environmental Research, Washington, DC, by research grants #HL 29845 and #HL 33177, National Institutes of Health, Bethesda, MD and by an Investigative Group Award by the Greater Los Angeles Affiliate of the American Heart Association, Los Angeles, CA. Dr. Brunken is the recipient of a Clinical Investigator Award (#HL 02022-02) from the National Institutes of Health, Bethesda, MD, and William Kuhle is the recipient of an American Heart Association Medical Student Research Fellowship.

REFERENCES

1. Tillisch J, Brunken R, Marshall R, et al. Reversibility of cardiac wall motion abnormalities predicted by positron tomography. *N Engl J Med* 1986;314:884–888.
2. Tamaki N, Yonekura Y, Yamashita K, et al. Positron emission tomography using fluorine-18 deoxyglucose in the evaluation of coronary artery bypass grafting. *Am J Cardiol* 1989;64:860–865.
3. Miller TR, Starren JB, Grothe RA. Three-dimensional display of positron emission tomography of the heart. *J Nucl Med* 1988;29:530–537.
4. Hicks K, Ganti G, Mullani N, Gould KL. Automated quantitation of three-dimensional cardiac positron emission tomography for routine clinical use. *J Nucl Med* 1989;30:1787–1797.
5. Kotzerke J, Hicks RJ, Wolfe E, et al. Three-dimensional assessment of myocardial oxidative metabolism: a new approach for regional determination of PET-derived carbon-11-acetate kinetics. *J Nucl Med* 1990;31: 1876–1893.
6. Berry JJ, Baker JA, Pieper KS, Hanson MW, Hoffman JM, Coleman RE. The effect of metabolic milieu on cardiac PET imaging using fluorine-18-deoxyglucose and nitrogen-13-ammonia in normal volunteers. *J Nucl Med* 1991;32:1518–1525.
7. Ratib O, Huang HK. CALIPSO: an interactive software package for multimodality medical image analysis on a personal computer. *J Med Imaging* 1989;3:205–216.
8. Kuhle WG, Porenta G, Huang S-C, Phelps ME, Schelbert HR. Issues in the quantitation of reoriented cardiac PET images. *J Nucl Med* 1992;33: 1235–1242.
9. Maddahi J, Van Train K, Prigent F, et al. Quantitative single photon emission computed thallium-201 tomography for detection and localization of coronary artery disease: Optimization and prospective validation of a new technique. *J Am Coll Cardiol* 1989;14:1689–1699.
10. Porenta G, Kuhle W, Sinha S, et al. Gated PET FDG imaging permits parameter estimation of cardiac geometry: validation using gated MR imaging and echocardiography [Abstract]. *J Nucl Med* 1991;32(suppl): 927.
11. Bonow RO, Dilsizian V, Cuocolo A, Bacharach SL. Identification of viable myocardium in patients with chronic coronary artery disease and left ventricular dysfunction. *Circulation* 1991;83:26–37.
12. Gould LK, Yoshida K, Hess MJ, Haynie M, Mullani N, Smalling RW. Myocardial metabolism of fluorodeoxyglucose compared to cell membrane integrity for the potassium analogue rubidium-82 for assessing infarct size in man. *J Nucl Med* 1991;32:1–9.
13. Wolpers HG, Geppert V, Hoeft A, Korb H, Schraeder R, Hellige G. Estimation of myocardial blood flow heterogeneity by transorgan helium transport functions. *Pflueg Arch* 1984;401:217–222.
14. Gropler RJ, Siegel BA, Lee KJ, et al. Nonuniformity in myocardial accumulation of fluorine-18-fluorodeoxyglucose in normal fasted humans. *J Nucl Med* 1990;31:1749–1756.
15. Choi Y, Brunken R, Hawkins R, et al. Determinants of myocardial glucose utilization assessed with dynamic FDG PET. *Circulation* 1991;84:II–425.
16. Knuuti MJ, Nuutila P, Ruotsalainen UH, et al. Euglycemic hyperinsulinemic clamp and oral glucose load in stimulating myocardial glucose utilization during positron emission tomography. *J Nucl Med* 1992;33: 1255–1262.